Electronic supplementary materials

Transfer relation between subgrade frost heave and slab track deformation and vehicle dynamic response in seasonally frozen ground

Juanjuan REN[1,2], Junhong DU[1,2], Kaiyao ZHANG[1,2], Bin YAN[3], Jincheng TIAN[4]

[1]*MOE Key Laboratory of High-speed Railway Engineering, Southwest Jiaotong University, Chengdu 610031, China*
[2]*School of Civil Engineering, Southwest Jiaotong University, Chengdu 610031, China*
[3]*School of Civil Engineering, Central South University, Changsha 410075, China*
[4]*Airport Planning and Design Institute, POWERCHINA Kunming Engineering Corporation Limited, Kunming 650051, China*

Section S1

The median data were used to define the distribution characteristics in the longitudinal direction, and a box plot of the time history curve of subgrade frost heaving was drawn to display the maximum, minimum, and median values of each group of data (Fig. S1). The values of subgrade frost heave in February at all measuring points were slightly greater than those in January, but the differences between the minimum, median, and maximum values of the two months were all within 1 mm, indicating the values detected in January and February were in line with the assumption of a stable freeze heave stage.

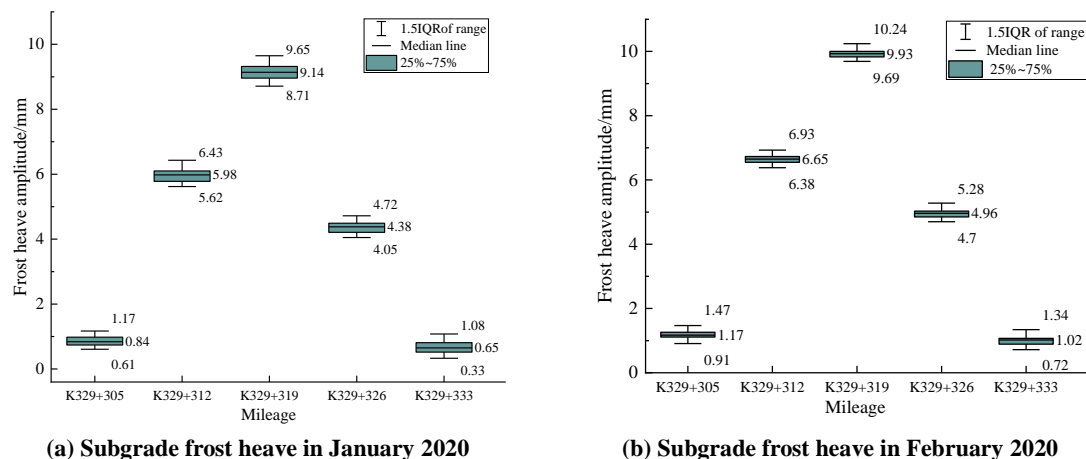(a) Subgrade frost heave in January 2020　　　(b) Subgrade frost heave in February 2020

Fig. S1　Box plot of subgrade frost heave deformation

The discrete points of the frost heave data have distribution characteristics similar to a Gaussian function and Fourier series. As such, the Gaussian function and Fourier series were selected for fitting, whose general expressions are Eqs. (S1) and (S2), respectively. Due to the

limited discrete data of frost heave, we adopted the finite–value Fourier series for data fitting (Awasthi, 2022).

$$f(x) = a\exp(-(x-b)^2 / 2c^2) \tag{S1}$$

$$f(x) = a_0 + \sum_{k=1}^{m}[a_k\cos(kwx) + b_k\sin(kwx)] \quad (m \le n/2) \tag{S2}$$

In Eq. (S1), a, b, and c are real number constants: a is the peak value of frost heaving, $x = b$ is the axis of symmetry of the Gaussian function, and c is the standard deviation. In Eq. (S2), a_0, a_k, and b_k are the Fourier coefficients and $w = 2\pi/L$, where L is the wavelength, k is the number of items, and x is the position coordinate. The coefficients of the fitting functions can be solved by the least square method (Hansen, et al., 2013). After fitting, the Gaussian and Fourier subgrade frost heave curves were expressed as:

$$f(x) = 10.08\exp(-(x-13.26)^2 / 9.308^2) \tag{S3}$$

$$f(x) = 5.559 - 4.406\cos(0.2196x) + 1.125\sin(0.2196x) \tag{S4}$$

The sum of squares due to error (SSE), determination coefficient (R–square), degree–of–freedom adjusted coefficient of determination (Adj R–sq), and root mean squared error (RMSE) of the fitted curves were extracted to evaluate the model fitting (Table S1). Compared with the Gaussian type, the SSE and RMSE values of the curve fitted by the Fourier series were closer to 0, and the R–square and Adj R–sq were closer to 1, indicating that the Fourier series provides more accurate results.

<center>Table S1   Subgrade frost heave curve fitting parameters</center>

Month	Parameter	Fitting function	
		Gaussian function	Fourier series
	SSE	0.4631	0.1542
February	R–square	0.9920	0.9973
	Adj R–sq	0.9840	0.9894
	RMSE	0.4812	0.3927

Section S2

The subgrade is composed of the surface layer of the subgrade bed, the bottom layer of the subgrade bed, and the embankment. For slab tracks on which high–speed trains with a speed of 350 km/h operate, the distance between the two tracks is 5 m, and the width of the subgrade surface is 13.6 m (NRAPRC, 2005). Because the subgrade of the double tracks is symmetrical about the vertical plane of the subgrade, we were able to reduce calculation workloads by building only half of the subgrade structure. Each layer of the subgrade was in common node contact. The material properties are shown in Table S2 (Zeng et al., 2019).

Table S2   Subgrade material properties

Layer	Height/m	Elastic modulus/GPa	Poisson's ratio (P)	Density/(kg m^{-3})	Damping ratio
Surface layer of subgrade bed	0.4	0.65	0.27	2430	0.028
Bottom layer of subgrade bed	2.3	0.47	0.32	2400	0.035
Embankment	2.3	0.47	0.32	2400	0.035

Classic cosine–type waveforms were selected as input conditions to validate the spatial coupling finite element model of CRTS III slab track–subgrade frost heave. For frost heave, the wavelengths were set as 10 m and 20 m, with an amplitude of 10 mm. We compared the calculation results with published data (Table S3).

Table S3   Comparison of simulation results with published data

Model	Rail displacement (mm)	SCC layer displacement (mm)	Base plate displacement (mm)	Debonding between SCC layer and base plate (mm)
Xu et al. (2019)– wavelength 20 m	10.105	10.229	10.235	0.133
This study– wavelength 20 m	10.753	11.227	11.126	0.574
Cai et al. (2021)–wavelength 10 m	10.425	–	–	0.380
This study – wavelength 10 m	10.091	10.944	10.903	0.296

Table S3 shows that the vertical displacements of the track layers in this study are similar to those from Cai et al. (2021), with an error rate within 10%. However, the results differ from those of Xu et al. (2019) in terms of debonding height. The reason is that the base plate of the model in this study used hard contact with the SCC layer, while that of Xu et al. (2019) adopted contact elements.

Section S3

To validate the dynamic model, the track irregularity spectrum of China's high–speed railway ballastless track (Lu et al., 2020) was used as the input excitation and expressed as:

$$S(f) = A / f^{k} \tag{S5}$$

where $S(f)$ is the power spectral density, f is the spatial frequency, and A and k are the coefficients of fitting (Table S4).

Table S4   Fitting coefficients of the ballastless track irregularity spectrum of the high–speed railway

	Section 1		Section 2		Section 3		Section 4	
	A	k	A	k	A	k	A	k
Height irregularity	1.05E–05	3.3891	3.56E–03	1.9271	1.98E–02	1.3643	1.99E–02	3.4516

The wavelength range of track irregularities was from 2 to 200 m, and the running speed was $V = 300$ km/h. Using a numerical simulation based on power spectrum sampling (Xu L, et al., 2022), the height irregularity of the ballastless track in the time domain can be obtained. The random track irregularity recommended by the Chinese Track Irregularity Spectrum of High–speed Railways Ballastless Track was used as the excitation for the wheel–rail system (Polach, 1999).

The cosine–type subgrade frost heave curve and track height irregularity were used as input conditions. The wavelength of the frost heave curve was 10 m, and the frost heaving amplitude was 10 mm. The analysis was performed in two steps, namely, import of the initial displacement, stress, and interlayer debonding calculated by the static model, and then dynamic calculation for the vehicle. Fig. S2 shows the calculation results of the vehicle dynamics, which were then compared with published data and the field test results (Table S5).
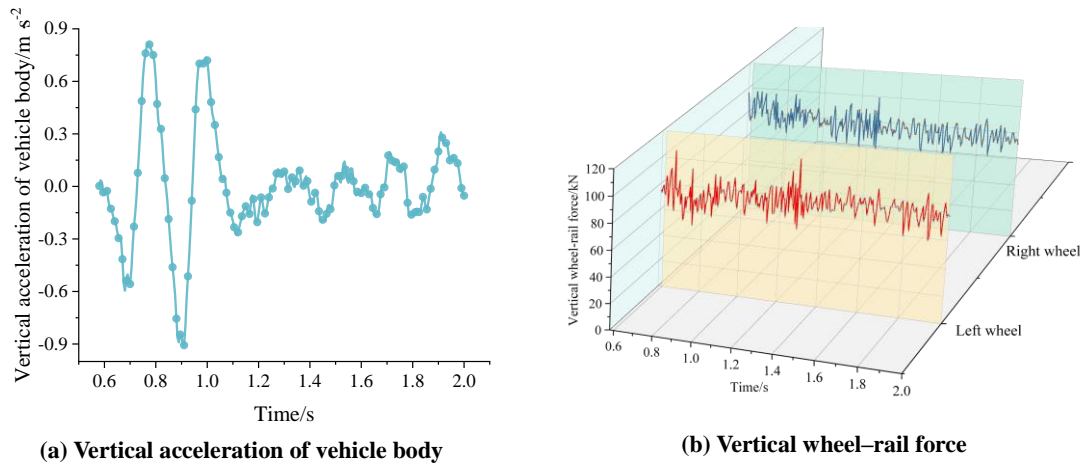

(a) Vertical acceleration of vehicle body   (b) Vertical wheel–rail force

Fig. S2   Dynamics calculation results

Table S5   Dynamics model validation

Dynamic response index	Model result	Cao et al. (2020) and Guo et al. (2015)	Field test results
Vehicle acceleration (m/s²)	–0.91~0.82	–0.6~0.6	–0.7~0.8
Peak of derailment coefficient	0.39	0.41	0.62

The simulation results of the vertical acceleration of the vehicle in this study were similar to those of other studies and field tests. The derailment coefficient was small because, in real–world operation, irregularity refers not just to height, but also to horizontal level and track gauge, causing the tested results to be larger than the simulation results. However, this was not considered in this study. Therefore, the discrepancy is understandable and does not undermine the reliability of the dynamic model.

References

Awasthi AK, Rachna, 2022. Fourier series and Fourier integral equations and their applications in elasticity. *Journal of Physics: Conference Series*, 2267:012158.
https://doi.org/10.1088/1742-6596/2267/1/012158

Guo J, Xu ZG, Sun YX, 2015. A new semi-active safety control strategy for high-speed railway vehicles. *Vehicle System Dynamics*, 53(12):1918-1934.
https://doi.org/10.1080/00423114.2015.1102297

Hansen PC, Pereyra V, Scherer G, 2013. Least Squares Data Fitting with Applications. Johns Hopkins University Press, Baltimore, USA, p.231-258.

Lu YH, Bi W, Zhang X, et al., 2020. Calculation method of dynamic loads spectrum and effects on fatigue damage of a full-scale carbody for high-speed trains. *Vehicle System Dynamics*, 58(7):1037-1056.
https://doi.org/10.1080/00423114.2019.1605080

MOR (Ministry of Railways of the People's Republic of China), 2005. Code for Design on Subgrade of Railway, TB 10001–2005. National Standards of the People's Republic of China (in Chinese).

Xu H, Cai WF, Wang P, 2019. Research on the influence of subgrade frost heave on CRTS III slab ballastless track. *Journal of Railway Engineering Society*, 36(10):27-32 (in Chinese).
https://doi.org/10.3969/j.issn.1006-2106.2019.10.006

Xu L, Zhao YS, Zhu ZX, et al., 2022. Vehicle-track random vibrations considering spatial frequency coherence of track irregularitives. *Vehicle System Dynamics*, 60(11):3977-3998.
https://doi.org/10.1080/00423114.2021.1986224

Zeng ZP, Wang JD, Shen SW, et al., 2019. Experimental study on evolution of mechanical properties of CRTS III ballastless slab track under fatigue load. *Construction and Building Materials*, 210:639-649.
https://doi.org/10.1016/j.conbuildmat.2019.03.080